Journal of Polymer Research (2023) 30:120
https://doi.org/10.1007/s10965-023-03484-1

ORIGINAL PAPER

Development of a novel silk sericin-based hydrogel film by mixture design

Natalia Jaramillo-Quiceno[1] · Santiago Rueda-Mira[1] · Juan Felipe Santa Marín[2] · Catalina Álvarez-López[1]

Received: 10 October 2022 / Accepted: 31 January 2023 / Published online: 28 February 2023

Abstract

Sericin has been used in functional and potentially biodegradable materials for cosmetics, biomedical, agricultural, and food applications. It is a natural polymer with applications in absorbent materials, such as hydrogels, because of its hydrophilic character. However, sericin by itself is brittle, and in contact with water has low structural stability, being necessary its blending with other polymers or the application of crosslinking processes. In this work, hydrogel films were prepared from different mixtures containing sericin (SS), carboxymethylcellulose (CMC), and polyvinyl alcohol (PVA), using a simple and environmentally friendly method consisting of a gelling process followed by solvent casting. A mixture design was applied to assess the incidence of each component and its interaction with the output variables of interest. Two response variables were evaluated in each formulation: water absorption capacity (WA) and gel fraction (GF). It was also possible to model the output variables based on the proportions of the sample components. In addition, a set of formulations were used to produce hydrogels with high water absorption rates while maintaining their structural stability. The optimal hydrogel formulation (HF) was structurally and thermally characterized by FTIR and TGA, respectively. Hydrogel morphology was also studied by scanning electron microscopy (SEM). The results of this study constitute an important contribution to the design of novel processing routes to extend the use of silk sericin in the development of new materials.

Keywords Silk sericin · Hydrogel film · Mixture design · Optimization · Carboxymethyl cellulose · Polyvinyl alcohol

Introduction

Hydrogels are hydrophilic materials, obtained by networks of cross-linked polymer that absorb and retain large amounts of water without solubilizing [1]. The presence of hydrophilic functional groups, such as -OH, -COOH, and -NH_2, gives hydrogels a high affinity with water [2], while their stability and flexibility are mainly a function of the crosslinking method used for their synthesis [3]. Chemical crosslinking produces strong covalent linkages (> 100 kJ/mol) between the polymer chains, meanwhile physical crosslinking gives rise to molecular entanglements and weak hydrogen and/or ionic bonds (only several kJ/mol) [2, 4].

Hydrogels may be formed in various arrangements, including matrixes, films, and microspheres [5]. From these, hydrogel films have gained importance in the development of functional membranes and coatings in several applications such as biosensors [6], drug-delivery systems, wound dressings [7], wastewater treatment [8], food packaging, slow-release fertilizers, and soil amendments [9]. They can be produced from synthetic monomers (e.g., acrylates, acrylamide), biorenewable polymers (polypeptides and polysaccharides), or their combination (semi-synthetic) [10]. Synthetic hydrogels contribute to environmental pollution [11, 12] because of their low biodegradability and possible toxicity. Hence, natural resources have been investigated as an alternative because they have hydrophilic properties, biodegradability, abundance, and low costs [13].

The use of some biopolymers, such as starch, can affect food safety [14], which is why a large part of the research in the area has been oriented to the exploration of natural polymers with low nutritional potential, such as alginate,

✉ Natalia Jaramillo-Quiceno
natalia.jaramilloq@upb.edu.co

[1] Grupo de Investigación Sobre Nuevos Materiales, Universidad Pontificia Bolivariana, Circular 1ª # 70-01, Medellín 050031, Colombia

[2] Grupo de Investigación Materiales Avanzados y Energía – MATyER, Instituto Tecnológico Metropolitano, Medellín, Colombia

chitosan, cellulose (and its derivates) and some proteins [15–18]. Among these, silk sericin (SS) is a promising protein for hydrogel film formulation. This silk biopolymer is composed mainly of polar amino acids with carboxyl and hydroxyl side chains [19]. Those molecules provide high water absorption capacity [20], and facilitate its crosslinking and mixing with other polymers for the design of biodegradable and structurally stable materials [21, 22].

Several sericin-based hydrogels have been developed combining this protein with other polymers such as carboxymethyl cellulose (CMC) [23, 24], sodium alginate [25], N-isopropyl acrylamide [26], and polyvinyl alcohol (PVA) [27–30]. PVA is a synthetic and biodegradable polymer extensively studied in mixtures with SS to manufacture flexible and structurally stable hydrogels [31, 32]. However, SS/PVA hydrogel films have a limited water absorption capacity, or, in most of the cases, it is necessary to use long and expensive processes to produce them (freeze-drying, freeze-thawing, salting out, or chemical crosslinking).

CMC is a hydrophilic polysaccharide with a large amount of hydroxy and carboxylic groups that promote physical crosslinking with other polymers, resulting in highly swellable, mechanically stable, and biodegradable materials [24, 33–35]. Moreover, several reports have shown that hydrogel films based on blends with CMC can be produced by simple and low-cost processes like solvent-casting [36–38]. However, to the best of the authors' knowledge, there are no studies that explore the addition of CMC into SS/PVA blends to develop hydrogel films with improved water absorption capacity.

Accordingly, the main objective of this work is to develop new sericin hydrogel materials from *Bombyx mori* L. defective cocoons by using a mixture design and response surfaces. The method was selected due to its effectiveness in optimizing blending processes. A new methodology to obtain hydrogel films, using silk protein in blending with CMC and PVA. CMC was considered in the hydrogel formulation to increase the water absorption capacity of SS/PVA blends. A simple and eco-friendly processing method was designed for hydrogel film formation, consisting of the cast drying of previously gelled SS/CMC/PVA blend. A response surface experiment was carried out to obtain an optimal hydrogel film composition (SS/CMC/PVA) with both maximum water absorption capacity and stability in water. Hydrogels obtained under the optimum conditions were characterized, and some types of interactions between polymers were elucidated.

Experimental

Materials

Colombian hybrid *Bombyx mori* L. defective cocoons (i.e., unreelable, double, stained, and pierced cocoons) were obtained from the Corporation for the Development of the Sericulture of Cauca – CORSEDA (Popayán, Colombia). Cocoons were air-dried and cut to remove the pupa and some impurities. Polyvinyl alcohol (PVA, MW: 146,000–186,000, 99% hydrolyzed, Sigma-Aldrich) and food-grade sodium carboxymethylcellulose (CMC, high viscosity 3500–4500 cP, degree of substitution: 0.7–0.9, Antioqueña de Químicos S.A.S) were used to obtain the films.

Extraction and concentration of silk sericin

Silk sericin (SS) was extracted using a high temperature and high pressure (HTHP) degumming method. Briefly, defective cocoons were cut into small pieces (around 5 mm), immersed in distilled water with a bath ratio of 1:30 (g of cocoons: ml of water), and then heated to 120 °C for 30 min in autoclave AV (Phoenix Ltda., Araraquara, Brazil). The obtained solution was filtered to remove fibroin fibers, resulting in a dilute aqueous sericin solution (~0.8% w/v). After that, a cryo-concentration procedure [39] was adopted to increase the amount of sericin in the solution. Accordingly, the dilute sericin solution was stored overnight in a closed container at room temperature. After this period, the hydrogel was frozen at -80 °C for 24 h and then was thawed at 35 °C for one h. The precipitated sericin was filtered and next solubilized by autoclaving at 120 °C for 15 min. The solution was adjusted by dilution into distilled water to get a sericin concentration of 2% w/v. The concentration of sericin in solutions obtained by both autoclave extraction (diluted) and cryo-concentration was confirmed by Biuret method [40] with a calibration curve made using a sericin commercial standard.

Experimental design

The effect of hydrogel composition (proportion in weight of X_1 – SS, X_2 – CMC, and X_3—PVA) on water absorption (g/g, Y_1) and gel fraction (%, Y_2) was evaluated using a three-component mixture design. This response surface experiment was performed due to its effectiveness in optimizing blending processes [41–43]. Specifically, a (3,3) simplex-lattice mixture design augmented with three axial data points was adopted, and the configuration of the resulting experiment is shown in Fig. 1. The final design included 13 points and a total of 78 runs (see Table 1). The experimental data were analyzed by Statgraphics Centurion XIX Version 19.1.2. A suitable mathematical model was fit for each response variable based on statistical parameters, such as multiple correlation coefficients (R^2, Adj. R^2) and p-value. The optimum hydrogel composition was selected with the highest water absorption and gel fraction using a numerical method based on desirability functions [41, 42]. The result was validated experimentally to confirm the model's reliability [44].

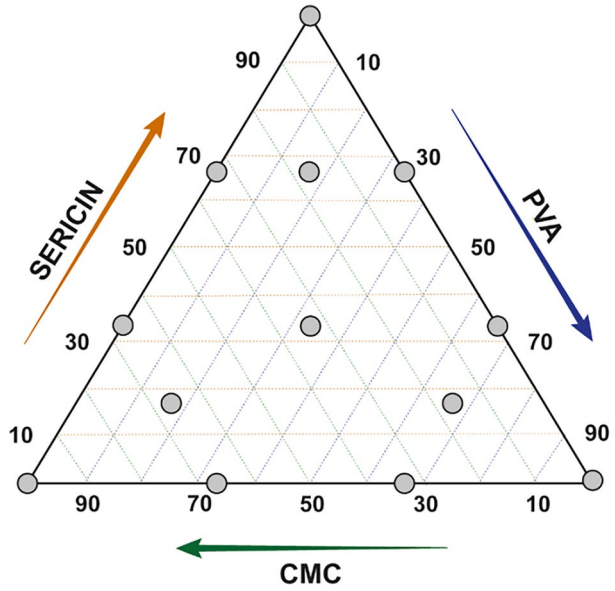

Fig. 1 Simplex-lattice design (3,3), augmented with three axial points, for three-component hydrogel film blends

Preparation of SS-CMC-PVA hydrogel films

The hydrogel blend was prepared according to the composition defined by each experimental point (Table 1). Initially, PVA was dissolved in distilled water at 85 °C with constant stirring for 2 h. The obtained PVA solution (1% w/v) was cooled to room temperature, and CMC was incorporated. The mixture was mechanically stirred for one hour at room temperature, followed by the addition of the concentrated SS solution (2% w/v) to reach a final volume of blend solution of 100 ml. The solution was stirred for 2 h to obtain a homogenous solution. The final SS/CMC/PVA blend (1.5% w/v) was poured into a plastic petri dish (90 mm diameter), left overnight at room temperature to remove air bubbles [36], and then dried in a hot air oven at 40 °C for 24 h to obtain the hydrogel films.

Determination of water absorption and gel fraction

Water absorption and gel fraction of hydrogel films were determined using the tea-bag method [45, 46]. A pre-weighted sample (50 mg) of dried samples was put in separate teabags and then immersed in distilled water (50 ml) at room temperature for 24 h. After this period, the bags were taken out of the water and weighed after carefully removing the excess water with a tissue. The test was performed in triplicate for each condition, and the water absorption was calculated using the following equation:

$$Water\ absorption\ (\%) = \left[\frac{W_S - W_0 - W_{TB}}{W_0}\right] \times 100 \quad (1)$$

where W_S represents the weight of sample and teabag in wet state, W_0 represents the weight of dry hydrogel, and W_{TB} relates to the weight of wet tea bag.

After water absorption test, the wet samples were dried at 60 °C until they reached a constant weight (W_d). The gel fraction of hydrogel films was determined as follows:

$$Gel\ fraction\ (\%) = \left[\frac{W_d}{W_0}\right] \times 100 \quad (2)$$

Table 1 Composition of the 13 experimental points of the simplex-lattice design (Fig. 1)

Exp point	Mass (g)		
	X_1 – SS	X2 – CMC	X3 – PVA
1	1.5	0	0
2	0	1.5	0
3	0	0	1.5
4	0.5	0.5	0.5
5	1.0	0.25	0.25
6	0.25	1.0	0.25
7	0.25	0.25	1.0
8	1.0	0.5	0
9	0.5	1.0	0
10	1	0	0.5
11	0.5	0	1
12	0	1.0	0.5
13	0	0.5	1.0

Characterization of hydrogel films

The hydrogel films were characterized by structural, thermal, and morphological properties. The infrared spectra of these samples were obtained using an Affinity1S (Shimadzu) Fourier Transform Infrared spectrophotometer with Attenuated Total Reflectance (FTIR-ATR) (SPECAC) accessory. Each spectrum was acquired in the range of 400 – 4000 cm^{-1}, performing 64 scans with a resolution of 4 cm^{-1}. Thermal stability was evaluated by thermogravimetry analysis using a Mettler–Toledo TGA/SDTA85 (TGA) device. The samples were heated from room temperature until 800 °C using a 10 °C/min ramp under an inert N_2 atmosphere. The morphology of the hydrogel films was examined using a scanning electron microscope SEM, JEOL 7100F at a voltage of 15 kV. Before the analysis, samples were prepared following the procedure described by previous reports [47] to maintain hydrogel porous structure integrity. Dried samples were dipped in distilled water for 24 h, frozen using liquid nitrogen, cryofractured, and then freeze-dried for 48 h. Lyophilized samples were treated by gold-sputtering before the microscopic examination. SEM images were analyzed using the open-sourced software ImageJ. A total of 100 measures of pore diameter were obtained per sample.

Results and discussion

Experimental design

Water absorption and gel fraction modeling: WA—GF

Table 2 shows the experimental design results used to study the effect of the ratio among the hydrogel components on the water absorption and gel fraction. The best fit model for all the response variables was the cubic, with the highest statistic Adj.R^2 and P-values < 0.05.

All significant coefficients below the 95% confidence level were eliminated, obtaining the following adjusted models for the response variables:

Water absorption

$$WA(g/g) = 1.1393X_1 + 1.657X_2 + 3.883X_3 + 97.147X_1X_2 - 10.229X_1X_3 + 88.721X_2X_3 + 172.783X_1X_2X_3 + 82.498X_1X_2(X_1 - X_2) \quad (3)$$

Gel fraction

$$GF(\%) = 82.388X_1 + 0.31012X_2 + 65.217X_3 - 101.638X_1X_2 + 26.763X_1X_3 + 61.408X_2X_3 + 592.726X_1X_2X_3 + 39.133X_1X_2(X_1 - X_2) + 0.124X_1X_3(X_1 - X_3) - 98.348X_2X_3(X_2 - X_3) \quad (4)$$

where WA and GF are the response variables, X_1, X_2, and X_3 are the SS, CMC, and PVA fractions in the hydrogel blend ($X_1 + X_2 + X_3 = 1$).

Positive and negative coefficients in both mathematical models revealed the existence of synergist and antagonistic effects, respectively [41, 48]. Double interaction between SS and PVA has an antagonist effect on water absorption due to the formation of a hydrogen bonds network between hydroxyl groups of PVA and the polar amino acid residues of SS. The formation of bonds could reduce the presence of hydrophilic functional groups and therefore decrease the swelling capacity of the hydrogel and enhance its stability in aqueous media [49, 50]. Accordingly, SS/PVA interaction resulted in a positive effect on the gel fraction model. Binary interactions of CMC with SS and PVA positively affected water absorption and, regarding gel fraction, had an antagonist effect. These findings suggest that the hygroscopic nature of CMC increases absorption capacity to the hydrogel network and, at the same time, promotes material dissolution in water.

Interestingly, ternary interactions showed a considerable positive effect in both adjusted models. Consequently, a more hydrophilic and stable network is obtained by the synergist effect of the SS/CMC/PVA blend. This result could be related to both electrostatic attractions between CMC (anionic polymer) and the protein chain [51, 52] and the formation of ion-dipolar complexes due to the interaction of the carboxylate anion of CMC with the hydroxyl group of PVA [38].

Table 2 Summary statistics for best fit models for water absorption and gel fraction responses

Response variable	Regression model	DF*	Sum of Squares	Mean Square	*F*-test	*P-value*	R^2	Adj. R^2
WA: water absorption	Cubic	7	8790	1256	26.34	0.0000	72.48	69.73
GF: gel fraction	Cubic	9	70,497	7833	477.97	0.0000	98.44	98.24

**DF* degrees of freedom

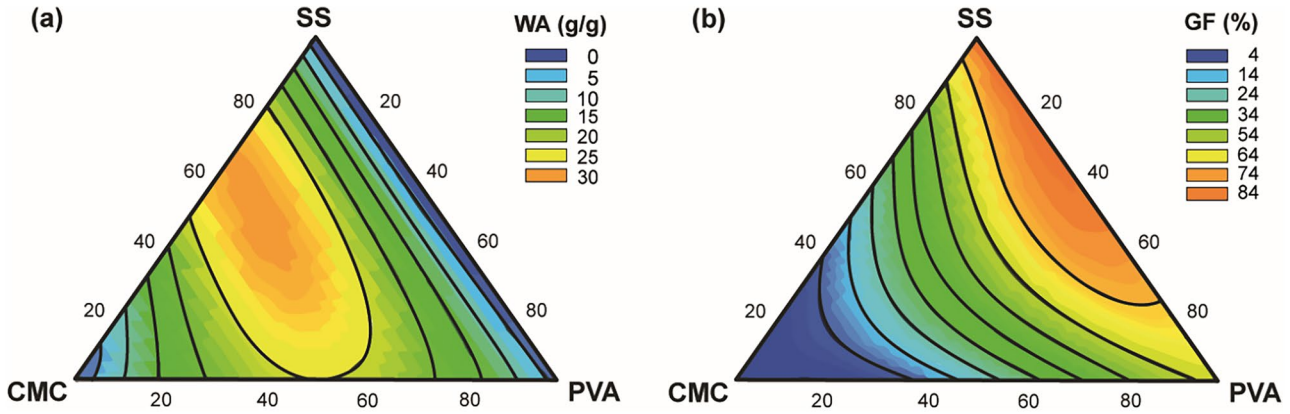

Fig. 2 Contour plots for the effect of different combinations of sericin (SS), carboxymethyl cellulose (CMC), and polyvinyl alcohol (PVA) on water absorption (**a**) and gel fraction (non-soluble fraction) (**b**) of film hydrogels

Further analysis of contour plots according to the adjusted models (Fig. 2) also showed that the CMC ratio strongly affects the water absorption response. Contour lines at extreme values of this component presented low WA, irrespective of the SS and PVA ratio (Fig. 2a). Therefore, an optimum region for the CMC ratio was found to be about 40 – 50%. Below this region, a significant presence of SS and PVA produces low water absorption. Meanwhile, at a CMC ratio above 50%, the structural integrity of the material network is reduced and, therefore, its absorption capacity. As shown in Fig. 2b, the non-soluble fraction in the hydrogel decreased when the CMC concentration increased. Moreover, the gel fraction contour plot suggests that SS and PVA promote CMC stabilization. The same behavior can be observed from the analysis of the adjusted model.

Optimization of the hydrogel formulation

A mathematical approach was used to obtain the best conditions for both optimization responses simultaneously. The model was based on the generation of desirability functions, and a value was assigned ranging from 0 to 1 to each predicted response [48, 53]. Then, overall desirability was obtained by geometric averaged individual desirability. Maximum water absorption and gel fraction values were defined as the desired criteria, and both response variables have the same weight in the optimization procedure [41]. Figure 3 presents the contour plot obtained for the overall desirability function, representing the optimal composition region as an orange area.

The optimal hydrogel formulation (HF) was composed of 45% of sericin, 25% CMC, and 30% PVA. Under these conditions, the model predicted a water absorption of 26.38 g/g and a gel fraction of 64.56%. The optimal results were validated experimentally, and the WA and GF were found to be 26.34 g/g and 62.14%, respectively. Accordingly, the error between the predicted value and the validation was 0.15% and 3.8% for WA and GF, respectively.

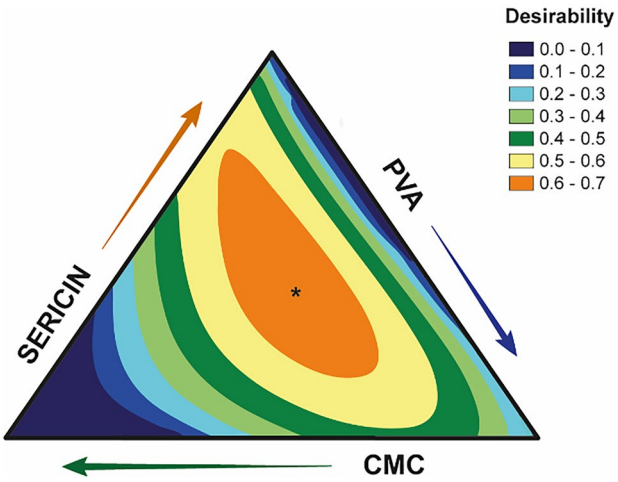

Fig. 3 Contour plot for desirability function for mixture design

Characterization of hydrogel films

Fourier transform infrared-attenuated total reflection spectroscopy

Figure 4 shows the FTIR spectrum obtained for the HF, SS, CMC, and PVA films. The spectra are in the range of (a) 3200 – 2700 cm^{-1}, (b) 1800 – 1300 cm^{-1}, and (c) 1200 – 800 cm^{-1}. In Fig. 4a, sericin film shows a strong absorption band between 3600 and 3200 cm^{-1} assigned to -OH and N–H stretching, and a higher intensity peak was observed at 3273 cm^{-1}, related by some authors to the degree of hydrogen bonding in β-sheet structures of SS films [54–56]. This last peak is shifted to 3275 cm^{-1} in the hydrogel film, indicating that the blending promotes hydrogen bonding interactions that change the resonance frequency of that kind of bond in the protein [27, 57].

CMC has a broad absorption band at 3360 cm^{-1} ascribed to intramolecular hydrogen bonds formed between O_6H_6 and COONa groups in the CMC chain [58]. The shifting of this band to a higher wavenumber (3393 cm^{-1}) in HF suggests that the hydrogen bond network of CMC was modified in the blending with SS and PVA. Moreover, this result could indicate that the blend has more interaction with water since it was previously reported that the peak at 3390 cm^{-1} is representative of the stretching mode of -OH groups in CMC bonded to water molecules [58]. Regarding pure PVA, there is a broad absorption band around 3285 cm^{-1} (O–H stretching) and the characteristic peaks of asymmetric and symmetric stretching of CH_2 at 2942 cm^{-1} and 2916 cm^{-1}, respectively [57, 59]. The infrared spectra of HF showed a band assigned to asymmetric stretching of CH_2 to shift to the left (2935 cm^{-1}), and the band at 2916 cm^{-1} is almost negligible.

The Amide I (1700–1600 cm-1) and Amide II (1600–1500 cm-1) bands were observed in the FTIR spectra of SS films (Fig. 4b). These bands are characteristic of FTIR protein spectrum; Amide I is directly related to the backbone conformation of proteins, reflecting C = O stretching vibration; and Amide II results from N–H and C-N vibrations. Therefore, the analysis of Amide I and Amide II bands has been commonly used for conformational studies of proteins like SS [60, 61]. Particularly, intense bands at 1620 cm^{-1} (stretching vibration of C = O) and 1520 cm^{-1} (N–H bending), as well as a shoulder at 1700 cm^{-1}. These bands evidenced that crystalline secondary structures (intermolecular hydrogen-bonded and intramolecular β-sheets) are predominant in SS films [60]. In the HF spectrum, the peaks at 1620 cm^{-1} and 1520 cm^{-1} are shifted to 1616 cm^{-1} and 1528 cm^{-1}, respectively. According to Barth and Sonjan et al. [27, 62], this result reveals the formation of hydrogen bonding between the protein and other polymers in the blend. The formation of this type of bond decreases the restoring force of C = O stretching vibrations (lowers resonance frequency) and produces an additional restoring force of N–H bending vibrations (increases resonance frequency) [62, 63].

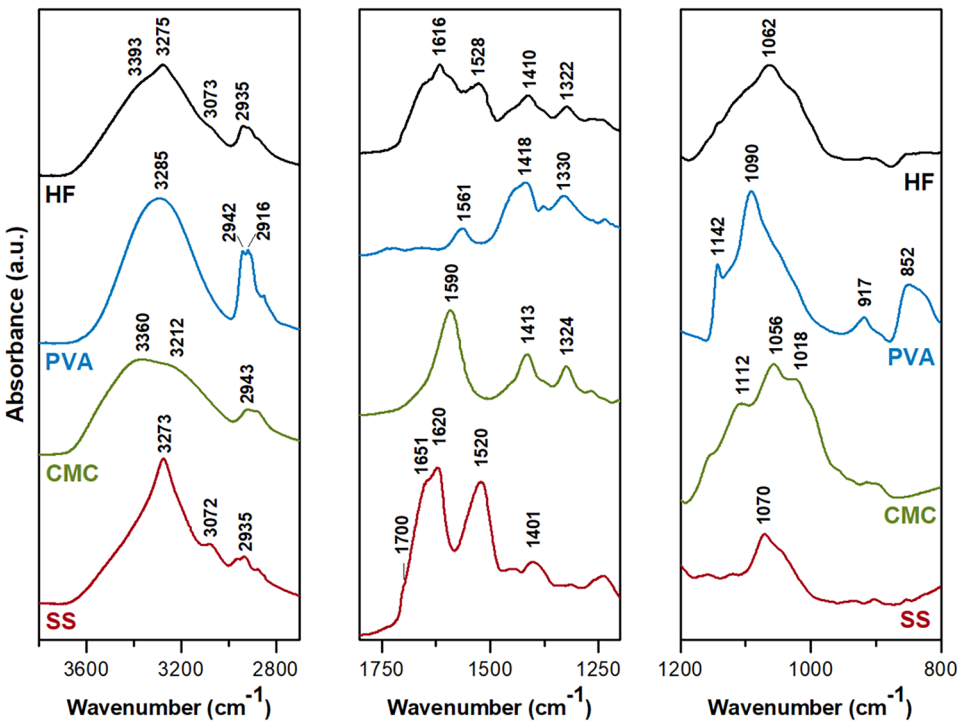

Fig. 4 FTIR spectrum for HF and neat SS, CMC, and PVA films in the range of (**a**) 3200 – 2700 cm^{-1}, (**b**) 1800 – 1200 cm^{-1}, and (**c**) 1200 – 800 cm^{-1}

The CMC spectrum shown in Fig. 4b has two bands related to the intramolecular forces of the carboxylate and hydroxyl group of this biopolymer. The first band is at 1590 cm^{-1} (asymmetrical vibration COO^{-}), and the second one is at 1324 cm^{-1} (bending vibration -OH) [38]. There is also a peak at 1413 cm^{-1} assigned to the scissoring vibration of -CH_2 groups. The intensity for the peak at 1590 cm^{-1} decreased in the HF spectrum, indicating the formation of intermolecular H-bonding likely between -COO^{-} of the CMC and -OH groups in the PVA [38] and the amino acid residues in SS (i.e., serine, threonine, and tyrosine) [54]. For PVA, there were three peaks at 1561 cm^{-1} (due to water absorption), 1418 cm^{-1} (CH_2 bending), and 1330 cm^{-1} (-CH wagging) [57]. Comparatively, the HF spectrum showed a reduction in the intensity of the band at 1418 cm^{-1}. Meanwhile, water absorption and -CH wagging vibration bands seem to be overlapped with the more intense bands of SS and CMC in this region.

Figure 4c shows that sericin has only one peak in the region between 1200 cm^{-1} and 800 cm^{-1}, found at 1070 cm^{-1}. It is ascribed to the stretching vibration of C–C and may be related to the high relative content of amino acid containing carboxylic acid (aspartic acid and glutamic acid) in silk sericin protein [64]. CMC spectrum (shown in Fig. 4c) exhibits a broad band centered at 1056 cm^{-1} (C–O–C bending vibrations). Although this band shifted to a higher wavenumber in HF (1062 cm-1), it is also the intensest band found in the blend at this range, suggesting a reordering in the molecular environment around C–O–C pyranose rings of CMC. The observed shift could result from the intermolecular hydrogen bonding formed by the interaction of the oxygen site in the ether linkage (C–O–C) and other molecules in polymer blending

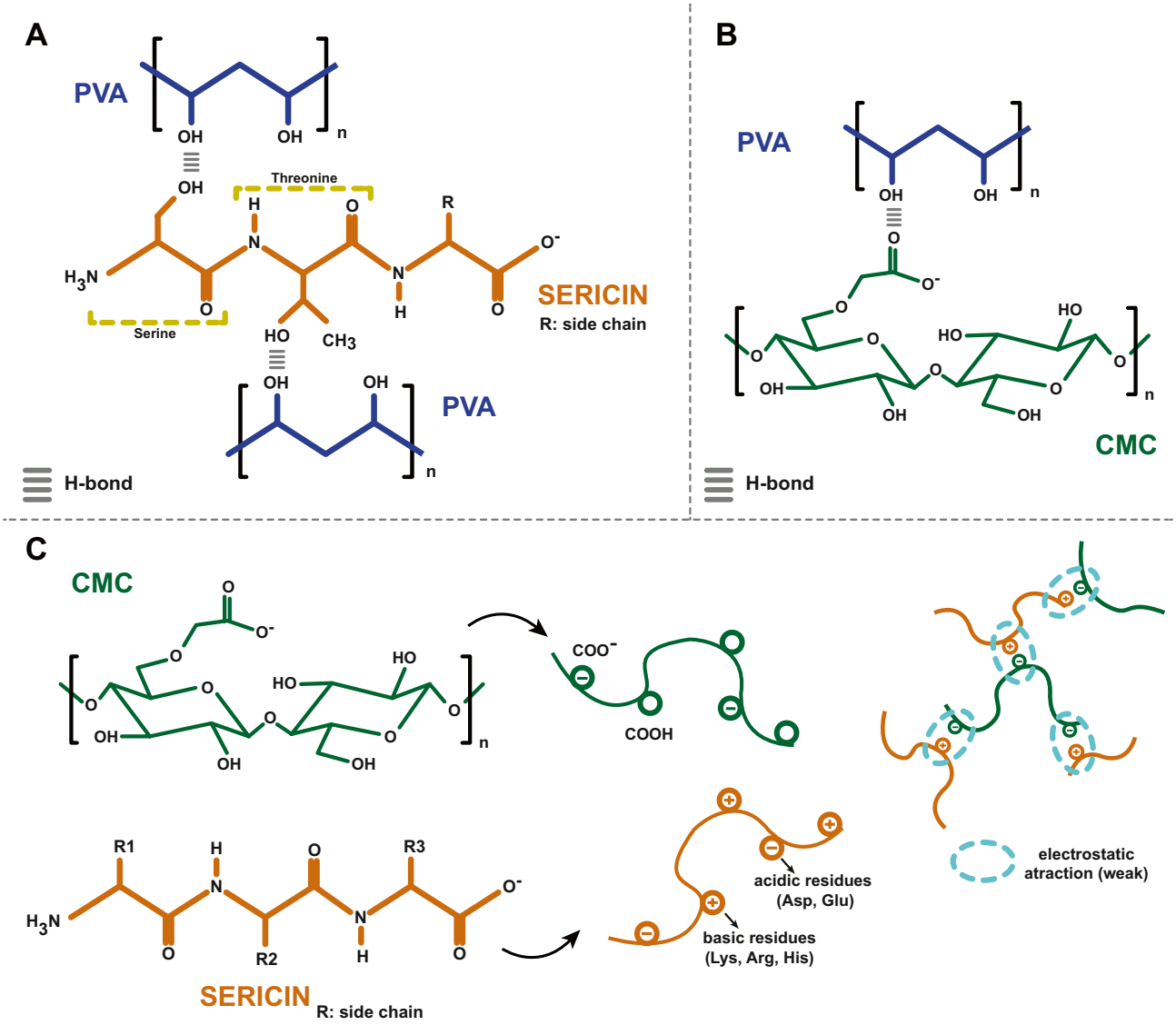

Fig. 5 Possible interaction mechanisms elucidated by FTIR analysis for (**A**) SS/PVA, (**B**) PVA/CMC and (**C**) SS/CMC

[38]. For PVA, two intense peaks at 1142 cm^{-1} (stretching of C-O) and 1090 cm-1 (stretching of C = O and bending of OH) were also observed, which related to the crystalline sequence of PVA [65]. Notably, the peak at 1142 cm^{-1} almost disappears in the HF spectra, indicating that H-bonding between polymers in the blending leads to a reduction of the crystalline fraction of PVA. Absorption bands in PVA spectra at 917 cm^{-1} (CH_2 rocking) and 852 cm^{-1} (C–C stretching) resulted almost negligible in HF spectra.

According to the results, it was concluded that no covalent interactions were obtained between the polymers in the hydrogel film. Moreover, these interactions seem to promote conformational changes in each component and elucidate the complexation by hydrogen bonding between the polymers in the blend [38]. Some of the interaction mechanisms described above are shown in Fig. 5.

Morphological analysis

SEM images were used to analyze the morphology of films formed with neat polymers: SS, CMC, PVA, 50/50 mixtures, and HF (Fig. 6). A non-porous structure was observed in the cross-section of SS film. This result suggests the presence of highly ordered and packed regions in the sample. These regions promoted the contraction process resulting in a dense and rough cross-section [66, 67]. As described before, SS films were obtained by a two-step process; stabilization (SS solution was left at room temperature for 24 h); and drying. It is believed that the ordered features typically obtained in SS films by the solvent casting method [60] may have increased due to the stabilization step. According to Reizabal et al. [68], this additional time is associated with a gelation process that favors the molecular reorganization of the protein and therefore its partial crystallization.

Conversely, both PVA and CMC hydrated films have tridimensional microstructures. PVA cross-sectional views reveal a porous network structure with an average pore size of around 1 µm. The observed porous structure results from the interaction of water with the amorphous PVA domains [69, 70]. In addition, the PVA network exhibits a significant pore density, indicating that the process used to obtain the film favors the arrangement of PVA molecules in ordered regions that act as knots of the network [69]. Besides, swollen CMC films show ribbon-like structures that shape spaces with an average diameter of around 26 µm. Ribbon-like structures denote polymer dissolution [71] and polymer network expansion due to water binding with the numerous hydroxyl and carboxyl groups in CMC. Moreover, wide interconnected spaces could be related to the electrostatic repulsion of CMC chains caused by the ionization of carboxyl groups during water immersion [35, 72].

Hydrated SS/CMC films have dense sheet-like structures with craters on them. The formation of nonporous planar aggregates could obey to poor interaction between the polymers, producing continuous regions of the protein separated by CMC chains that bind to water and then, during freeze-drying, create the observed spaces between the sheets [73]. As proposed by the FTIR analysis, electrostatic attractions between polar amino acids in SS and -COO^- groups seemed to govern the interaction between SS and CMC. However, the low degree of interaction revealed by the SEM micrographs could be related to the presence of negatively charged amino acids that can limit electrostatic attraction between these polymers.

SS/PVA and CMC/PVA mixtures exhibited a homogeneous porous structure with an average pore diameter of around 1 µm and 20 µm, respectively. This result confirms the physical crosslinking of PVA with both SS and CMC

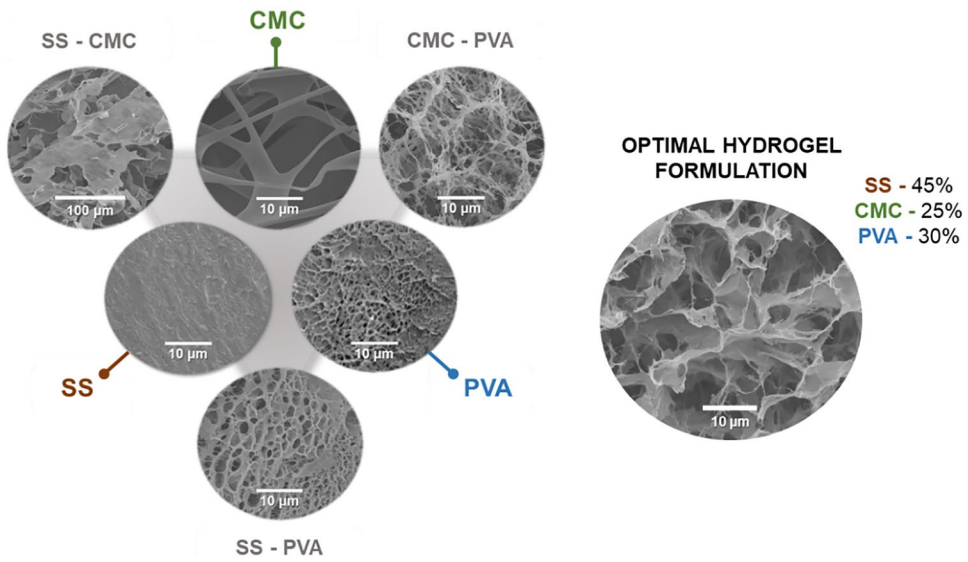

Fig. 6 SEM images of neat SS, CMC, and PVA, 50/50 mixtures, and optimal hydrogel formulation films

Table 3 Summary of the morphological analysis ($n = 100$)

Type of hydrogel film	Average pore size (µm)	Morphology
SS	N/A	Non-porous
CMC	26.3 ± 14.7	Ribbon-like structures
PVA	1.1 ± 0.4	Porous
SS/PVA	1.0 ± 0.8	Homogeneous pores
SS/CMC	N/A	Nonporous planar aggregates
CMC/PVA	6.2 ± 4.5	Homogeneous pores
HF	8.3 ± 5.1	Mixture: Homogeneous pores with sheet-like walls

via hydrogen bonding [35, 74], as described in the FTIR analysis. However, pore density in the CMC/PVA is lower than that observed in SS/PVA films. These results could be related to a low degree of crosslinking in the CMC/PVA system. The differences in pore diameter could be explained by the fact that swollen CMC molecules repeal each other during swelling in water, producing the expansion of the three-dimensional network.

The porous network observed for the optimal hydrogel formulation combines morphological features observed in the 50/50 mixtures. The average pore size in HF is around 8 µm; the interconnected pore structure reveals the formation of crosslinking points, possibly due to hydrogen bonding, electrostatic attractions (SS/CMC), and ion-dipolar complexes (CMC/PVA). The formation of these pore layers could be explained by the remaining interaction between SS and CMC that promotes the formation of planar structures. Consequently, the structure that arises from the HF (45:25:30 for SS:CMC:PVA proportions) likely promotes swelling capacity and stability in an aqueous medium, which is consistent with the results obtained in the mixture optimization study. Table 3 resumes the results of the morphological analysis. From these, it is possible to confirm the effect of the synergistic interactions between the polymers in the optimal hydrogel film formulation.

Thermogravimetric analysis

Thermogravimetric analysis (TGA) and derivative (DTG) of individual polymers, 50/50 blends, and the optimal hydrogel formulation (HF) are presented in Fig. 7A-D. All the neat polymers (SS, CMC, and PVA) showed a slight weight loss (6—13%) before 200 °C (Fig. 7A, C). This first degradation step was associated with free and bound water evaporation. From these individual polymers, CMC exhibited the lowest temperature of water removal (69 °C) and a significant weight loss before 200 °C (13%), suggesting that free water content in this sample was higher than SS and PVA due to the high absorption capacity of CMC [38, 75].

According to the DTG curves for individual polymers (Fig. 7C), SS seems to degrade in a wide range (226 to 470 °C), with a maximum degradation temperature (T_{max}) of 308 °C. This behavior could be related to subsequent decomposition reactions during heating, like the elimination of volatile compounds, the breakdown of side chain groups of amino acid residues, and the cleavage of polypeptide bonds [61, 76]. Although SS also exhibited a first degradation peak at 255 °C and a shoulder at 233 °C, there are no reports that associate specific degradation mechanisms with their appearance. However, the degradation pattern of the SS film obtained in this study differs from the ones reported for sericin obtained with different extraction and concentration processes [61, 77]. CMC exhibits two degradation steps between 248 and 333 °C; at around 256 °C, a more significant weight loss was observed (29%), related to the rupture of -COO groups and C–C bonds of CMC (decarboxylation reaction). Between 270 and 333 °C, breaking strong bonds in the polymer backbone leads to final CMC decomposition [78]. Meanwhile, the characteristic degradation of PVA chains occurred almost in a single step at a T_{max} of 260 °C with a weight loss of (70%).

From 50/50 blends thermograms (see Fig. 7B, D), all the samples showed a first weight loss before 200 °C. The weight loss was higher for SS/CMC and CMC/PVA (~ 12%) than for SS/PVA (7%), confirming the incidence of CMC in the water absorption capacity of a polymer blend with SS and PVA. After weight loss, 50/50 blends started to degrade, and the T_{max} of CMC/PVA and SS/PVA blends were higher than those of the neat polymers. This improvement in thermal stability is associated with the occurrence of physical crosslinking reactions between the polymers [78], as corroborated by the FTIR analysis. Moreover, SS/PVA showed the highest degradation temperature (324 °C), which is related to the high degree of crosslinking observed in the morphological analysis of this sample. Conversely, SS/CMC blend exhibit a lower T_{max} (291 °C) than that of the SS film (308 °C), underlining that weak interaction between SS and CMC leads to a decrease in the thermal stability of SS in the blending.

Optimal hydrogel formulation film (HF) (see Fig. 7B, D) had a weight loss before 200 °C (6%) comparable to that obtained for SS/PVA blend (7%). Moreover, the maximum degradation temperature of this sample was 301 °C, which is close to that of SS and higher than that of PVA or CMC. However, SS/PVA blend seems to have major thermal stability than HF, implying that CMC incorporation into SS/PVA blend could affect the inter and intramolecular interactions between the polymers. This corroborates the FTIR and SEM analysis findings, particularly the physical crosslinking of the polymers in the blend and the major affinity between SS and PVA.

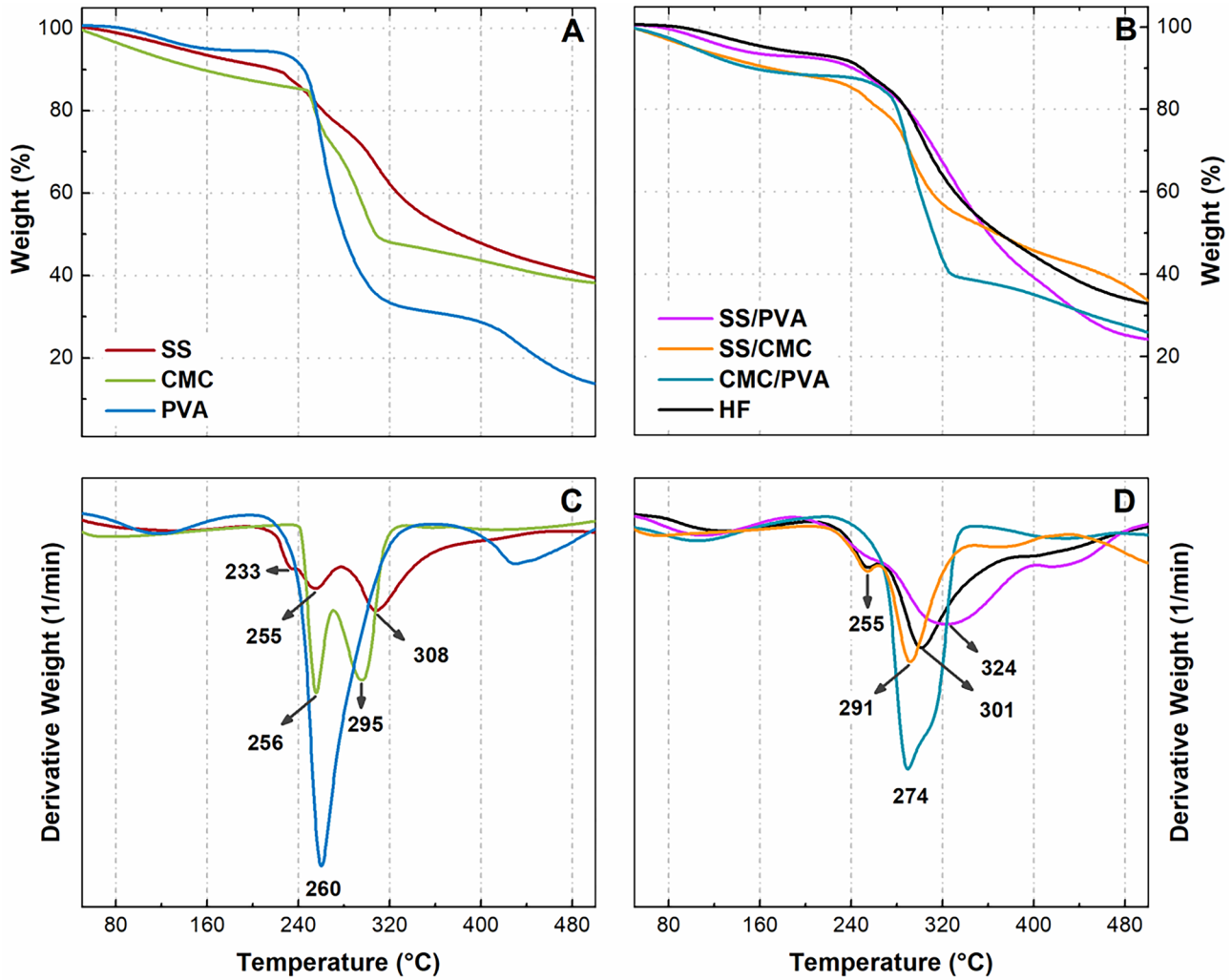

Fig. 7 TGA (**A** and **B**) and DTG (**C** and **D**) curves for neat polymers, 50/50 blends, and optimal hydrogel formulation films

Conclusions

The formulation of a hydrogel film based on SS/CMC/PVA blending was optimized by a response surface design. A mathematical approach was used to obtain the best conditions for optimization responses (water absorption—WA and gel fraction—GF). The optimal hydrogel formulation (HF) was composed of 45% of sericin, 25% CMC, and 30% PVA. This means that around 70% of the developed material consists of natural sources, making it potentially biodegradable.

According to the adjusted models for WA and GF, physical crosslinking mechanisms dominate the formation of the three-dimensional network of the HF. It was evidenced that interactions between SS and PVA lead to a decrease in swelling capacity and enhance structural stability. Regarding CMC, it could be suggested that electrostatic attractions domain its interaction with SS, while the formation of ion-dipolar complexes is related to CMC/PVA bonding formation. In any case, the non-crosslinked fraction of CMC seems to promote material dissolution in water.

These findings were coherent with the characterization results. FTIR suggested the occurrence of complexation by hydrogen bonding between the polymers in the HF blend, leading to conformational changes, especially in SS and PVA. The morphology analysis of HF revealed the formation of a polymer network with an average pore size of around 8 µm. Crosslinking points and planar structures forming the porous structure of HF were related to non-covalent interactions and the remaining interaction between SS and CMC, respectively.

Thermogravimetric (TGA) results indicate that binary and ternary blend promotes thermal stability. Since SS/PVA blend showed a higher T_{max} (324 °C) than that observed in HF (301 °C) and, it was suggested that CMC incorporation in SS/PVA could affect inter and intramolecular bonding, reducing thermal stability.

The overall results demonstrate the potential of response surface methodology for optimizing polymer blends and, even more, the understanding of the mechanisms involved. Moreover, the successful implementation of a novel processing method (gelation followed by solvent casting) to fabricate hydrogel films could boost the development of low-cost and environmentally friendly sericin-based absorbent materials.

Acknowledgements The authors would like to acknowledge the Ministerio de Ciencia, Tecnología e Innovación (MINCIENCIAS), for its financial support through the Ph.D. Grant 785 of 2017 and the research grant 127-2021 for the program "Tecnologías en Agricultura Urbana", Convocatoria MINCIENCIAS 852, 2019. This program was funded by resources from PATRIMONIO AUTÓNOMO FONDO NACIONAL DE FINANCIAMIENTO PARA LA CIENCIA, LA TECNOLOGÍA Y LA INNOVACIÓN FRANCISCO JOSÉ DE CALDAS.

Author contribution Conceptualization, NJQ, CAL; methodology, NJQ, JFS, and CAL; investigation, NJQ, SRM, JFS, and CAL; resources, CAL and JFS; data curation, NJQ; writing—original draft preparation, NJQ, and CAL; writing—review and editing, NJQ, JFS, and CAL; visualization, NJQ; supervision, CAL and JFS; funding acquisition, NJQ, and CAL.

Funding This study was financially supported by Ministerio de Ciencia, Tecnología e Innovación (MINCIENCIAS) (Ph.D. Grant 785 of 2017 and Research Grant 127–2021). Open Access funding provided by Colombia Consortium.

Declarations

Conflict of interest The authors declare that they have no known competing financial interests or personal relationships that could have appeared to influence the work reported in this paper.

References

1. Hoffman A (2012) Hydrogels for biomedical applications. Adv Drug Deliv Rev 64:18–23. https://doi.org/10.1016/j.addr.2012.09.010
2. Liu Y, Wang J, Chen H, Cheng D (2022) Environmentally friendly hydrogel: A review of classification, preparation and application in agriculture. Sci Total Environ 846:157303. https://doi.org/10.1016/j.scitotenv.2022.157303
3. Chen Y (2020) Properties and development of hydrogels. In: Chen Y (ed) Hydrogels Based on Natural Polymers. Elsevier, pp 3–16
4. Mignon A, de Belie N, Dubruel P, van Vlierberghe S (2019) Superabsorbent polymers: A review on the characteristics and applications of synthetic, polysaccharide-based, semi-synthetic and 'smart' derivatives. Eur Polym J 117:165–178. https://doi.org/10.1016/j.eurpolymj.2019.04.054
5. Ahmed EM (2015) Hydrogel: Preparation, characterization, and applications: A review. J Adv Res 6:105–121. https://doi.org/10.1016/j.jare.2013.07.006
6. Kaniewska K, Karbarz M, Katz E (2020) Nanocomposite hydrogel films and coatings – Features and applications. Appl Mater Today 20:100776. https://doi.org/10.1016/j.apmt.2020.100776
7. Divyashri G, Badhe R, v., Sadanandan B, et al (2022) Applications of hydrogel-baseddelivery systems in wound care and treatment: An up-to-date review. Polym Adv Technol 33:2025–2043. https://doi.org/10.1002/pat.5661
8. van Tran V, Park D, Lee YC (2018) Hydrogel applications for adsorption of contaminants in water and wastewater treatment. Environ Sci Pollut Res 25:24569–24599
9. Klein M, Poverenov E (2020) Natural biopolymer-based hydrogels for use in food and agriculture. J Sci Food Agric 100:2337–2347. https://doi.org/10.1002/jsfa.10274
10. Ramli RA (2019) Slow release fertilizer hydrogels: A review. Polym Chem 10:6073–6090. https://doi.org/10.1039/c9py01036j
11. Demitri C, Scalera F, Madaghiele M et al (2013) Potential of cellulose-based superabsorbent hydrogels as water reservoir in agriculture. Int J Polym Sci
12. Azeredo H, Waldron K (2016) Crosslinking in polysaccharide and protein films and coatings for food contact - A review. Trends Food Sci Technol 52:109–122. https://doi.org/10.1016/j.tifs.2016.04.008
13. Guilherme M, Aouada FA, Fajardo AR et al (2015) Superabsorbent hydrogels based on polysaccharides for application in agriculture as soil conditioner and nutrient carrier: a review. Eur Polym J 72:365–385. https://doi.org/10.1016/j.eurpolymj.2015.04.017
14. Luo MT, Li HL, Huang C et al (2018) Cellulose-based absorbent production from bacterial cellulose and acrylic acid: Synthesis and performance. Polymers (Basel) 10. https://doi.org/10.3390/polym10070702
15. Skrzypczak D, Witek-Krowiak A, Dawiec-Liśniewska A et al (2019) Immobilization of biosorbent in hydrogel as a new environmentally friendly fertilizer for micronutrients delivery. J Clean Prod 241. https://doi.org/10.1016/j.jclepro.2019.118387
16. Feng D, Bai B, Wang H, Suo Y (2017) Novel fabrication of biodegradable superabsorbent microspheres with diffusion barrier through thermo-chemical modification and their potential agriculture applications for water holding and sustained release of fertilizer. J Agric Food Chem 65:5896–5907. https://doi.org/10.1021/acs.jafc.7b01849
17. Kong W, Li Q, Li X et al (2019) A biodegradable biomass-based polymeric composite for slow release and water retention. J Environ Manage 230:190–198. https://doi.org/10.1016/j.jenvman.2018.09.086
18. Calabria L, Vieceli N, Bianchi O et al (2012) Soy protein isolate/poly(lactic acid) injection-molded biodegradable blends for slow release of fertilizers. Ind Crops Prod 36:41–46. https://doi.org/10.1016/j.indcrop.2011.08.003
19. Zhang Y-Q (2002) Applications of natural silk protein sericin in biomaterials. Biotechnol Adv 20:91–100. https://doi.org/10.1016/S0734-9750(02)00003-4
20. Gupta D, Agrawal A, Chaudhary H et al (2013) Cleaner process for extraction of sericin using infrared. J Clean Prod 52:488–494. https://doi.org/10.1016/J.JCLEPRO.2013.03.016
21. Dash BC, Mandal BB, Kundu SC (2009) Silk gland sericin protein membranes: fabrication and characterization for potential

biotechnological applications. J Biotechnol 144:321–329. https://doi.org/10.1016/j.jbiotec.2009.09.019
22. da Silva TL, da Silva AC, Vieira MGA et al (2016) Biosorption study of copper and zinc by particles produced from silk sericin – alginate blend: evaluation of blend proportion and thermal cross-linking process in particles production. J Clean Prod 137:1470–1478. https://doi.org/10.1016/j.jclepro.2015.05.067
23. Nayak S, Kundu S (2014) Sericin-carboxymethyl cellulose porous matrices as cellular wound dressing material. J Biomed Mater Res A 102:1928–1940. https://doi.org/10.1002/jbm.a.34865
24. Siritientong T, Aramwit P (2015) Characteristics of carboxymethyl cellulose/sericin hydrogels and the influence of molecular weight of carboxymethyl cellulose. Macromol Res 23:861–866. https://doi.org/10.1007/s13233-015-3116-z
25. Zhang Y, Liu J, Huang L et al (2015) Design and performance of a sericin-alginate interpenetrating network hydrogel for cell and drug delivery. Sci Rep 5:1–13. https://doi.org/10.1038/srep12374
26. Zhang Q, Dong P, Chen L et al (2014) Genipin-cross-linked thermosensitive silk sericin/poly(N- isopropylacrylamide) hydrogels for cell proliferation and rapid detachment. J Biomed Mater Res A 102:76–83. https://doi.org/10.1002/jbm.a.34670
27. Sonjan S, Ross GM, Mahasaranon S et al (2021) Biodegradable hydrophilic film of crosslinked PVA/silk sericin for seed coating: the effect of crosslinker loading and polymer concentration. J Polym Environ 29:323–334. https://doi.org/10.1007/s10924-020-01867-9
28. Aramwit P, Siritientong T, Kanokpanont S, Srichana T (2010) Formulation and characterization of silk sericin-PVA scaffold crosslinked with genipin. Int J Biol Macromol 47:668–675. https://doi.org/10.1016/j.ijbiomac.2010.08.015
29. Aramwit P, Siritienthong T, Srichana T, Ratanavaraporn J (2013) Accelerated healing of full-thickness wounds by genipin-crosslinked silk sericin/PVA scaffolds. Cells Tissues Organs 197:224–238. https://doi.org/10.1159/000345600
30. Aramwit P, Ratanavaraporn J, Ekgasit S et al (2015) A green salt-leaching technique to produce sericin/PVA/glycerin scaffolds with distinguished characteristics for wound-dressing applications. J Biomed Mater Res B Appl Biomater 103:915–924. https://doi.org/10.1002/jbm.b.33264
31. Tao G, Wang Y, Cai R et al (2019) Design and performance of sericin/poly(vinyl alcohol) hydrogel as a drug delivery carrier for potential wound dressing application. Mater Sci Eng, C 101:341–351. https://doi.org/10.1016/j.msec.2019.03.111
32. Wang F, Li Z, Guo J et al (2022) Highly strong, tough, and stretchable conductive hydrogels based on silk sericin-mediated multiple physical interactions for flexible sensors. ACS Appl Polym Mater 4:618–626. https://doi.org/10.1021/acsapm.1c01553
33. Wang P, He H, Cai R et al (2019) Cross-linking of dialdehyde carboxymethyl cellulose with silk sericin to reinforce sericin film for potential biomedical application. Carbohydr Polym 212:403–411. https://doi.org/10.1016/j.carbpol.2019.02.069
34. Capanema NSV, Mansur AAP, de Jesus AC et al (2018) Superabsorbent crosslinked carboxymethyl cellulose-PEG hydrogels for potential wound dressing applications. Int J Biol Macromol 106:1218–1234. https://doi.org/10.1016/j.ijbiomac.2017.08.124
35. Xiao C, Gao Y (2008) Preparation and properties of physically crosslinked sodium carboxymethylcellulose/poly(vinyl alcohol) complex hydrogels. J Appl Polym Sci 107:1568–1572. https://doi.org/10.1002/app.27203
36. Ghorpade VS, Dias RJ, Mali KK, Mulla SI (2019) Citric acid crosslinked carboxymethylcellulose-polyvinyl alcohol hydrogel films for extended release of water soluble basic drugs. J Drug Deliv Sci Technol 52:421–430. https://doi.org/10.1016/j.jddst.2019.05.013
37. Esteghlal S, Niakousari M, Hosseini SMH (2018) Physical and mechanical properties of gelatin-CMC composite films under the influence of electrostatic interactions. Int J Biol Macromol 114:1–9. https://doi.org/10.1016/j.ijbiomac.2018.03.079
38. Saadiah MA, Zhang D, Nagao Y et al (2019) Reducing crystallinity on thin film based CMC/PVA hybrid polymer for application as a host in polymer electrolytes. J Non Cryst Solids 511:201–211. https://doi.org/10.1016/j.jnoncrysol.2018.11.032
39. Vidart JMM, Silva TL da, Rosa PCP et al (2018) Development of sericin/alginate particles by ionic gelation technique for the controlled release of diclofenac sodium. J Appl Polym Sci 135:45919. https://doi.org/10.1002/app.45919
40. Arango MC, Osorio YM, Osorno JB et al (2022) Effect of Ethanol Post-Treatments over Sericin Scaffolds for Tissue Engineering Applications. J Polym Environ. https://doi.org/10.1007/s10924-022-02647-3
41. Gutiérrez H, de la Vara R, Cano A et al (2008) Análisis y diseño de experimentos. Mc Graw-Hill
42. Montgomery D (2009) Design and analysis of experiments. Wiley, Hoboken, NJ
43. Ly O, Monchau F, Rémond S et al (2020) Optimization of the formulation of an original hydrogel-based bone cement using a mixture design. J Mech Behav Biomed Mater 110:1–8. https://doi.org/10.1016/j.jmbbm.2020.103886
44. Hu Q, Lin H, Wang Y et al (2021) Design, optimization and evaluation of a microemulsion-based hydrogel with high malleability for enhanced transdermal delivery of levamisole. Int J Pharm 605:120829. https://doi.org/10.1016/j.ijpharm.2021.120829
45. Zhang K, Feng W, Jin C (2020) Protocol efficiently measuring the swelling rate of hydrogels. MethodsX 7:100779. https://doi.org/10.1016/j.mex.2019.100779
46. Mohammadi-Khoo S, Moghadam PN, Fareghi AR, Movagharnezhad N (2016) Synthesis of a cellulose-based hydrogel network: characterization and study of urea fertilizer slow release. J Appl Polym Sci 133:1–9. https://doi.org/10.1002/app.42935
47. Qiao D, Liu H, Yu L et al (2016) Preparation and characterization of slow-release fertilizer encapsulated by starch-based superabsorbent polymer. Carbohydr Polym 147:146–154. https://doi.org/10.1016/j.carbpol.2016.04.010
48. Costa RDO, Coutinho JP, Santos RLSR (2022) Use of mixture design to optimize nanofabrication of dithiocarbazate–loaded polylactic acid nanoparticles. J Appl Polym Sci 139:51504. https://doi.org/10.1002/app.51504
49. He H, Cai R, Wang Y et al (2017) Preparation and characterization of silk sericin/PVA blend film with silver nanoparticles for potential antimicrobial application. Int J Biol Macromol 104:457–464. https://doi.org/10.1016/j.ijbiomac.2017.06.009
50. Thangprasert A, Tansakul C, Thuaksubun N, Meesane J (2019) Mimicked hybrid hydrogel based on gelatin/PVA for tissue engineering in subchondral bone interface for osteoarthritis surgery. Mater Des 183:108113. https://doi.org/10.1016/j.matdes.2019.108113
51. Li Z, Wang Y, Pei Y et al (2017) Effect of substitution degree on carboxymethylcellulose interaction with lysozyme. Food Hydrocoll 62:222–229. https://doi.org/10.1016/j.foodhyd.2016.07.020
52. Duhoranimana E, Karangwa E, Lai L et al (2017) Effect of sodium carboxymethyl cellulose on complex coacervates formation with gelatin: Coacervates characterization, stabilization and formation mechanism. Food Hydrocoll 69:111–120. https://doi.org/10.1016/j.foodhyd.2017.01.035
53. Didier C, Etcheverrigaray M, Kratje R, Goicoechea HC (2007) Crossed mixture design and multiple response analysis for developing complex culture media used in recombinant protein production. Chemom Intell Lab Syst 86:1–9. https://doi.org/10.1016/j.chemolab.2006.07.007
54. Kumkun P, Tuancharoensri N, Ross G et al (2019) Green fabrication route of robust, biodegradable silk sericin and poly(vinyl alcohol) nanofibrous scaffolds. Polym Int 68:1903–1913. https://doi.org/10.1002/pi.5900

55. Yooyod M, Ross GM, Limpeanchob N et al (2016) Investigation of silk sericin conformational structure for fabrication into porous scaffolds with poly(vinyl alcohol) for skin tissue reconstruction. Eur Polym J 81:43–52. https://doi.org/10.1016/j.eurpolymj.2016.05.023
56. Krimm S, Bandekar J (1986) Vibrational spectroscopy and conformation of peptides, polypeptides, and proteins. Adv Protein Chem 38:181–364. https://doi.org/10.1016/S0065-3233(08)60528-8
57. Jipa I, Stoica A, Stroescu M et al (2012) Potassium sorbate release from poly(vinyl alcohol)-bacterial cellulose films. Chemical Papers 66. https://doi.org/10.2478/s11696-011-0068-4
58. Li W, Sun B, Wu P (2009) Study on hydrogen bonds of carboxymethyl cellulose sodium film with two-dimensional correlation infrared spectroscopy. Carbohydr Polym 78:454–461. https://doi.org/10.1016/j.carbpol.2009.05.002
59. Zeng P, Chen X, Qin YR et al (2019) Preparation and characterization of a novel colorimetric indicator film based on gelatin/polyvinyl alcohol incorporating mulberry anthocyanin extracts for monitoring fish freshness. Food Res Int 126. https://doi.org/10.1016/j.foodres.2019.108604
60. Jaramillo-Quiceno N, Callone E, Dirè S et al (2021) Boosting sericin extraction through alternative silk sources. Polym J 53:1425–1437. https://doi.org/10.1038/s41428-021-00539-2
61. Arango MC, Álvarez-López C (2019) Effect of freezing temperature on the properties of lyophilized silk sericin scaffold. Mater Res Express 6. https://doi.org/10.1088/2053-1591/ab3594
62. Barth A (2007) Infrared spectroscopy of proteins. Biochim Biophys Acta Bioenerg 1767:1073–1101. https://doi.org/10.1016/j.bbabio.2007.06.004
63. Colthup N (2012) Introduction to infrared and Raman spectroscopy. Elsevier
64. Zhang X, Wyeth P (2010) Using FTIR spectroscopy to detect sericin on historic silk. Sci China Chem 53:626–631. https://doi.org/10.1007/s11426-010-0050-y
65. Ou K, Dong X, Qin C et al (2017) Properties and toughening mechanisms of PVA/PAM double-network hydrogels prepared by freeze-thawing and anneal-swelling. Mater Sci Eng, C 77:1017–1026. https://doi.org/10.1016/j.msec.2017.03.287
66. Puerta M, Peresin MS, Restrepo-Osorio A (2020) Effects of chemical post-treatments on structural and physicochemical properties of silk fibroin films obtained from silk fibrous waste. Front Bioeng Biotechnol 8. https://doi.org/10.3389/fbioe.2020.523949
67. Zhang C, Song D, Lu Q et al (2012) Flexibility regeneration of silk fibroin in vitro. Biomacromol 13:2148–2153. https://doi.org/10.1021/bm300541g
68. Reizabal A, Costa CM, Saiz PG et al (2021) Processing strategies to obtain highly porous silk fibroin structures with tailored microstructure and molecular characteristics and their applicability in water remediation. J Hazard Mater 403. https://doi.org/10.1016/j.jhazmat.2020.123675
69. Ricciardi R, Auriemma F, De Rosa C, Lauprêtre F (2004) X-ray Diffraction Analysis of Poly(vinyl alcohol) Hydrogels, Obtained by Freezing and Thawing Techniques. Macromolecules 37:1921–1927. https://doi.org/10.1021/ma035663q
70. Fumio U, Hiroshi Y, Kumiko N et al (1990) Swelling and mechanical properties of poly(vinyl alcohol) hydrogels. Int J Pharm 58:135–142. https://doi.org/10.1016/0378-5173(90)90251-X
71. Wang C, Tian M, Xin Y et al (2019) Self-supporting three-dimensional carboxymethyl cellulose conductive sponges used as electrodes for lithium-ion batteries. Cellulose 26:8025–8036. https://doi.org/10.1007/s10570-019-02644-1
72. BeMiller JN (2019) Cellulose and Cellulose-Based Hydrocolloids. In: Carbohydrate Chemistry for Food Scientists. Elsevier, pp 223–240
73. Lin X, Jin J, Guo X, Jia X (2021) All-carboxymethyl cellulose sponges for removal of heavy metal ions. Cellulose 28:3113–3122. https://doi.org/10.1007/s10570-021-03685-1
74. Aramwit P, Sereemaspun A, Yamdech R (2018) Sericin ameliorates the properties of poly(vinyl alcohol) hydrogel prepared by simple repeated freeze-thaw process without the use of chemical crosslinking. Int J Res Sci 4:6. https://doi.org/10.24178/ijrs.2018.4.3.06
75. Yazawa K, Ishida K, Masunaga H et al (2016) Influence of Water Content on the β-Sheet Formation, Thermal Stability, Water Removal, and Mechanical Properties of Silk Materials. Biomacromol 17:1057–1066. https://doi.org/10.1021/acs.biomac.5b01685
76. Padasalagi AB, Rabinal MHK (2022) Controlled emission of carbon quantum dots derived from waste silk sericin. Part Part Syst Charact 39:2200041. https://doi.org/10.1002/ppsc.202200041
77. Castrillón Martínez D, Zuluaga CL, Restrepo-Osorio A, Álvarez-López C (2017) Characterization of sericin obtained from cocoons and silk yarns. Procedia Eng 200:377–383. https://doi.org/10.1016/j.proeng.2017.07.053
78. Harun-or-Rashid MD, Saifur Rahaman MD, Enamul Kabir S, Khan MA (2016) Effect of hydrochloric acid on the properties of biodegradable packaging materials of carboxymethylcellulose/poly(vinyl alcohol) blends. J Appl Polym Sci 133:n/a-n/a. https://doi.org/10.1002/app.42870